

Embed to rigorously and accurately homogenise quasi-periodic multi-scale heterogeneous PDEs, with computer algebra

A. J. Roberts *

September 8, 2022

Abstract

For microscale heterogeneous PDEs, this article further develops novel theory and methodology for their macroscale mathematical/asymptotic homogenization. This article specifically encompasses the case of quasi-periodic heterogeneity with finite scale separation: no scale separation limit is required. Dynamical systems theory frames the homogenization as a slow manifold of the ensemble of all phase-shifts of the heterogeneity. Depending upon any perceived scale separation *within* the quasi-periodic heterogeneity, the homogenization may be done in either one step, or two sequential steps: the results are equivalent. The theory not only assures us of the existence and emergence of the homogenization, it also provides a practical systematic method to construct the homogenization to any specified order. For a class of heterogeneities, we show that the macroscale homogenization is potentially valid down to lengths which are just twice that of the microscale heterogeneity! This methodology provides a new rigorous and flexible approach to homogenization that potentially also provides correct initial and boundary conditions, treatment of forcing and control, and analysis of uncertainty.

*University of Adelaide, South Australia. <http://orcid.org/0000-0001-8930-1552>,
<mailto:profajroberts@protonmail.com>

Contents

1	Introduction	2
2	Phase-shift embedding	6
3	The slow manifold of homogenization	9
3.1	Spectrum at each equilibrium	10
3.2	Results of slowly varying theory	12
4	Example construction of homogenized PDE	13
4.1	Iteration systematically constructs	14
5	Spatial resolution of homogenization	16
6	Three-scale homogenization	21
6.1	Meso-slow homogenization	21
6.2	Homogenization of the mesoscale model	24
7	Conclusion	25
A	Computer algebra to construct an homogenized PDE	26
A.1	Quickly verify a leading approximation	27
A.2	Iteration systematically constructs	27
B	Meso-scale homogenization code	30

1 Introduction

Many engineering and scientific structures have microscale structure, such as lattice materials (e.g., [Somnic & Jo 2022b,a](#), [Barchiesi et al. 2020](#)), the windings in electrical machinery (e.g., [Romanazzi et al. 2016](#)), electromagnetism in micro-structured material (e.g., [Craster 2015](#), [Niyonzima 2014](#)), food drying (e.g., [Welsh et al. 2018](#)), and slow Stokes flow through porous media (e.g., [Brown et al. 2011](#)). The engineering challenge is to understand the dynamics on a scale significantly larger than the micro-structure. Homogenization, via the recognition of multiple physical length scales, is the common approach¹. This article further develops a new approach to modelling the large scale homogenized dynamics via a newly established general rigorous theory ([Roberts](#)

¹(e.g., [Gustafsson & Mossino 2003](#), [Engquist & Souganidis 2008](#), [Cooper 2018](#), [Abdulle & Pouchon 2020](#))

2015a, §2.5). This new approach provides a route to systematic refinements of the homogenization, without any of the usual assumptions except a *finite* separation of scales, and to novel quantification of the remainder error.

Consider materials with complicated microstructure: we want to model their large scale dynamics by equations with effective, ‘average’ coefficients. Heterogeneous diffusion in 1D is the simplest such example: suppose the material, in spatial domain $[0, L]$, has structure so that ‘material’ or ‘heat’ $u(t, x)$ diffuses according to

$$\frac{\partial u}{\partial t} = \frac{\partial}{\partial x} \left\{ \kappa(x) \frac{\partial u}{\partial x} \right\}, \quad 0 < x < L, \quad (1)$$

where the heterogeneous diffusion coefficient $\kappa(x)$ has some complicated multiscale structure. For definiteness, let’s initially suppose the macroscale boundary conditions are simply that u is L -periodic in space x . Our challenge is to derive the model PDE

$$\frac{\partial U}{\partial t} = K \frac{\partial^2 U}{\partial x^2} + \dots \quad (2)$$

for some effective mean field $U(x, t)$, some effective macroscale diffusivity K , with some higher order corrections (\dots), and possibly an error estimate (\dots). We also comment throughout on the closely related problem² of wave propagation through heterogeneous material, $u_{tt} = \partial_x \{ \kappa(x) u_x \}$, and its corresponding effective homogenized PDE models $U_{tt} = KU_{xx} + \dots$ that predict its macroscale dispersive waves.

Here we focus on cases where the heterogeneity $\kappa(x)$ is quasi-periodic in space. For example, [Sections 4](#) and [5](#) focuses on homogenization for the family of heterogeneous diffusivities $\kappa = 1/[1 + a_1 \cos(2\pi x/\ell_1) + a_2 \cos(2\pi x/\ell_2)]$ for arbitrary microscale periods ℓ_1, ℓ_2 with $\ell_1 > \ell_2$. [Sections 2](#) and [3](#) develops theory and supporting characteristics of homogenization in the general case where the heterogeneity κ is expressible as a function of two variables, say $\kappa(x_1, x_2)$, in which κ is ℓ_i -periodic in variable x_i . Then the quasi-periodic heterogeneity in [\(1\)](#) is $\kappa(x, x)$.

Almost all extant conventional approaches to homogenization depend upon the identification of a *representative volume element* (RVE) (e.g., [Somnic & Jo 2022a](#)), or a representative cell. Even in the simple case of periodic media an uncertain issue is an appropriate size of an RVE³. An issue with

²(e.g., [Shahraki & Guzina 2020](#), [Cornaggia & Guzina 2020](#), [Abdulle & Pouchon 2020](#))

³(e.g., [Nguyen et al. 2011](#), [Saeb et al. 2016](#), [Matouš et al. 2017](#), [Klarmann et al. 2019](#), [Schneider 2021](#), [Somnic & Jo 2022b](#), §2.3, §1.2.2, §5.1, p.2, p.2, p.13, resp.)

such RVE-like approaches is that for quasi-periodic heterogeneities there is *no* one RVE (e.g., [Anthoine 2010](#), §2.1). When the microscale lengths ℓ_1, ℓ_2 are irrationally related, then all volume elements, no matter what size is chosen, are different: no volume element is representative. Relatedly, when the microscale lengths ℓ_1, ℓ_2 have a large least common multiple, then any true RVE must be large—unnecessarily large. Instead [Sections 2 and 3](#) develop a novel a rigorous approach that, in effect, uses an ‘RVE’ which is the size of the largest microscale length, albeit of more spatial dimensions.

I expect straightforward extensions of the approach developed herein to empower cognate analysis and modelling of the following:

- cases where the heterogeneity is quasi-periodic in any number of microscale lengths $\ell_1 > \ell_2 > \ell_3 > \dots$;
- PDEs [\(1\)](#) where the field u is itself in a vector space such as the cross-sectional structure of either shear dispersion (e.g., [Mercer & Roberts 1990, 1994](#)), or of elastic beams (e.g., [Roberts 1993](#));
- multiple macroscale space dimensions as in the modelling of plates and shells (e.g., [Roberts & Bunder 2017](#));
- PDEs like [\(1\)](#) but with macroscale variations in the material parameters as well as microscale variations (e.g., [Anthoine 2010](#))—sometimes called *functionally graded materials*;
- PDEs like [\(1\)](#) but with nonlinear effects (e.g., [Matouš et al. 2017](#)).

Here we significantly extend the new approach to modelling the multiscale class of systems where notionally both microscales $\ell_1, \ell_2 \ll L$, the macroscale length. But the [Section 6](#) shows that the analysis and results also include three-scale multiscale systems where notionally $\ell_2 \ll \ell_1 \ll L$, that is, where there is a microscale, a mesoscale, and a macroscale⁴.

Analytic techniques such as mathematical homogenization or the method of multiple scales⁵ provide a mechanism for deriving effective PDE models such as [\(2\)](#). But such previous underlying theory requires the limit of infinite scale separation between the microscale ‘cell’-sizes ℓ_i and the macroscale domain size L ⁶. In contrast, and arising from developments in dynamical systems, [Sections 2 and 3](#) respectively use phase-shift embedding and slowly varying theory ([Roberts 2015a, Roberts & Bunder 2017](#)) to provide rigorous support

⁴(e.g., [Ramirez-Torres et al. 2018, Cruz-González et al. 2022](#))

⁵(e.g., [Shahraki & Guzina 2020, Cornaggia & Guzina 2020](#))

⁶(e.g., [Welsh et al. 2018, Barchiesi et al. 2020, Altmann et al. 2021](#), p.5, §2.4 & p.6, resp.)

to the modelling at finite scale separation: that is, when the macroscale length scale L is larger than the microscales ℓ_1 and ℓ_2 , but not infinitely so. In the approach here, not only is there no limit, there is no need for a defined “ ϵ ”. Such finite scale separation empowers this approach to capture the dispersion in wave homogenization which [Abdulle & Pouchon \(2020\)](#) call for in their discussion [p.3] that “new effective models are required”. The phase-shift embedding developed here further illustrates the general principle that macroscale models of microscale structures are often best phrased as ensemble averages⁷.

It is well recognised that homogenization is physically effective for reasonably well separated length scales: that the resolved macroscale structures, with length ℓ_M say, satisfy $\ell_M \gg \ell_1$. But what does this mean? Much extant homogenization theory requires the mathematical limit $\ell_1/\ell_M \rightarrow 0$. However, *physically* the ratio ℓ_1/ℓ_M is always finite. By setting homogenization on a new rigorous footing, [Section 5](#) analyses homogenization to high-order and presents evidence that, in a class of problems, a *quantitative* limit to the spatial resolution of homogenization is that $\ell_1/\ell_M \lesssim 1/2$, equivalently $\ell_M \gtrsim 2\ell_1$. Mathematically, a wider scale separation is not necessary for homogenization.

Of course, practically we usually prefer a wider scale separation because of many complicating factors in construction and use of practical homogenization models. But, in the sense discussed by [Section 5](#), this quantitative lower bound on the required scale separation indicates how little scale separation is necessary. Indeed, because it applies at finite scale separation, the analysis here encompasses *high-contrast media* and so also detects features occurring in this particularly interesting class of problems (e.g., [Cooper 2018](#), p.2).

The new approach to homogenization that we develop here creates a powerful dynamical systems framework for addressing other modelling issues in the future. For a time-dependent simulation of homogenized dynamics one must provide some initial conditions for the PDE [\(2\)](#). These initial conditions are surprisingly nontrivial at finite scale separation, but the new framework developed here comes with well-established methods to derive the correct initial conditions for long-term forecasts⁸. The projection that provides the correct initial conditions, also provides the correct projection of any applied ‘forcing’ ([Roberts 1989](#), §7), including the cases of control, and system uncertainty. System uncertainty is a challenge for other techniques⁹. Further, the homog-

⁷(e.g., [van Kampen 1992](#), [Drugan & Willis 1996](#), [Birch & Young 2006](#))

⁸(e.g., [Roberts 1989](#), [1993](#), [Cox & Roberts 1995](#), [Roberts 2000](#))

⁹(e.g., [Matouš et al. 2017](#), [Altmann et al. 2021](#), §8 & p.3, resp.)

enized PDE (2) needs boundary conditions—a “highly challenging problem” according to [Shahraki & Guzina \(2020\)](#), and which [Cornaggia & Guzina \(2020\)](#) called a “complex problem that is still an active research topic”. Such boundary conditions are nontrivial, but again the new framework developed here comes with a rigorous approach to derive correct boundary conditions for accurate predictions at finite scale separation¹⁰. That is, this approach to homogenization potentially provides a rational complete modelling of not just the PDE at finite scale separation, but also material variations, uncertainty, control, forcing, and initial and boundary conditions. In their review of nonlinear homogenization, [Matouš et al. \(2017\)](#) [§8] commented that “verification ensures both order of accuracy and consistency . . . even mathematical foundations for verification are lacking”—the approach developed here provides the required mathematical foundation.

The approach herein has no need of a variational formulation of the governing equations¹¹, and so applies to a much wider class of problems than many homogenization methods.

Throughout this article, in the details of the construction of homogenizations, one may observe that the variables x_0, x_1, x_2 appear in much the same sort of algebraic expressions traditionally obtained by the method of multiple scales. What this parallelism implies is that in suitable circumstances the algebraic machinations of the method of multiple scales are indeed sound. What is new here is that we place such algebraic details in a new and more rigorous framework. The new framework developed here provides clarity, precision, power, and greater physical interpretability to homogenization.

2 Phase-shift embedding

Let’s embed the specific given PDE (1) into a family of PDE problems formed by all phase-shifts of the quasi-periodic microscale. This embedding is a novel and rigorous twist to the concept of a *representative volume element*.

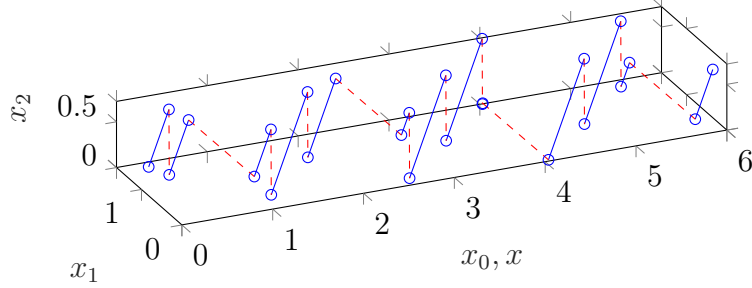
As indicated by [Figure 1](#), let’s create the desired embedding by considering a field $\mathbf{u}(t, x_0, x_1, x_2)$ satisfying the PDE

$$\frac{\partial \mathbf{u}}{\partial t} = \left(\frac{\partial}{\partial x_0} + \frac{\partial}{\partial x_1} + \frac{\partial}{\partial x_2} \right) \left\{ \kappa(x_1, x_2) \left(\frac{\partial \mathbf{u}}{\partial x_0} + \frac{\partial \mathbf{u}}{\partial x_1} + \frac{\partial \mathbf{u}}{\partial x_2} \right) \right\} \quad (3)$$

¹⁰(e.g., [Roberts 1992, 1993](#), [Mercer & Roberts 1994](#), [Chen et al. 2014, 2015, 2018](#))

¹¹(e.g., [Barchiesi et al. 2020](#), [Altmann et al. 2021](#), §2.4 & §3, resp.)

Figure 1: schematic cylindrical domain \mathcal{D} of the multiscale embedding PDE (3) for a field $\mathbf{u}(t, x_0, x_1, x_2)$ (here $L = \ell_0 = 6$, $\ell_1 = 1.62$, $\ell_2 = 0.72$). We obtain solutions of the heterogeneous diffusion PDE (1), or (4), on such blue lines as $u(t, x) = \mathbf{u}(t, x, x + \phi_1, x + \phi_2)$ for every pair of constant phases ϕ_1 and ϕ_2 (here $\phi_1 = 0.82$ and $\phi_2 = 0.32$), and where the last two arguments of \mathbf{u} are modulo ℓ_1 and ℓ_2 , respectively.



in the domain $\mathcal{D} := \{(x_0, x_1, x_2) : x_i \in [0, \ell_i]\}$, for the macroscale $\ell_0 = L$ and microscale ℓ_1, ℓ_2 , and with ℓ_i -periodic boundary conditions in x_i . We define $\kappa_{\min} := \min_{x_i \in [0, \ell_i]} \kappa(x_1, x_2)$, and assume $\kappa_{\min} > 0$. The domain \mathcal{D} in $x_0x_1x_2$ -space (Figure 1) is often termed *cylindrical* as it is long and thin. I emphasise that this domain has finite aspect ratio: we do *not* take any limit involving an aspect ratio tending to zero nor to infinity.

Figure 1 indicates that we consider $x_0 = x$. The distinction between x_0 and x is that partial derivatives in x_0 are done keeping the other x_i constant, whereas partial derivatives in x are done keeping the phases ϕ_i constant.

Lemma 1. *For every solution $\mathbf{u}(t, x_0, x_1, x_2)$ of the embedding PDE (3), and for every vector of phases $\boldsymbol{\phi} := (\phi_1, \phi_2)$, the field $u_{\boldsymbol{\phi}}(t, x) := \mathbf{u}(t, x, x + \phi_1, x + \phi_2)$ (that is, the field \mathbf{u} evaluated on the solid-blue lines in Figure 1) satisfies the heterogeneous diffusion PDE*

$$\frac{\partial u_{\boldsymbol{\phi}}}{\partial t} = \frac{\partial}{\partial x} \left\{ \kappa(x + \phi_1, x + \phi_2) \frac{\partial u_{\boldsymbol{\phi}}}{\partial x} \right\}. \quad (4)$$

Hence the field $u(t, x) := \mathbf{u}(t, x, x, x)$ satisfies the given heterogeneous PDE (1).

Recall that the most common boundary conditions assumed for RVEs are periodic, whereas here the ℓ_1, ℓ_2 -periodic boundary conditions are not assumed but arise naturally due to the ensemble of phase-shifts. That is, what previously had to be assumed, here arises naturally.

Proof. Start by considering the left-hand side time derivative in PDE (4):

$$\begin{aligned}
\frac{\partial u_\phi}{\partial t} &= \frac{\partial}{\partial t} \mathbf{u}(t, x, x + \phi_1, x + \phi_2) \\
&= \left[\frac{\partial \mathbf{u}}{\partial t} \right]_{(t, x, x + \phi_1, x + \phi_2)} \quad (\text{which by PDE (3) becomes}) \\
&= \left[\left(\frac{\partial}{\partial x_0} + \frac{\partial}{\partial x_1} + \frac{\partial}{\partial x_2} \right) \left\{ \kappa(x_1, x_2) \left(\frac{\partial \mathbf{u}}{\partial x_0} + \frac{\partial \mathbf{u}}{\partial x_1} + \frac{\partial \mathbf{u}}{\partial x_2} \right) \right\} \right]_{(t, x, x + \phi_1, x + \phi_2)} \\
&= \frac{\partial}{\partial x} \left\{ \left[\kappa(x_1, x_2) \left(\frac{\partial \mathbf{u}}{\partial x_0} + \frac{\partial \mathbf{u}}{\partial x_1} + \frac{\partial \mathbf{u}}{\partial x_2} \right) \right]_{(t, x, x + \phi_1, x + \phi_2)} \right\} \\
&= \frac{\partial}{\partial x} \left\{ \kappa(x + \phi_1, x + \phi_2) \left[\frac{\partial \mathbf{u}}{\partial x_0} + \frac{\partial \mathbf{u}}{\partial x_1} + \frac{\partial \mathbf{u}}{\partial x_2} \right]_{(t, x, x + \phi_1, x + \phi_2)} \right\} \\
&= \frac{\partial}{\partial x} \left\{ \kappa(x + \phi_1, x + \phi_2) \frac{\partial}{\partial x} \mathbf{u}(t, x, x + \phi_1, x + \phi_2) \right\} \\
&= \frac{\partial}{\partial x} \left\{ \kappa(x + \phi_1, x + \phi_2) \frac{\partial u_\phi}{\partial x} \right\},
\end{aligned}$$

namely the right-hand side of (4). Hence, provided PDE (3) has boundary conditions of ℓ_i -periodicity in x_i , every solution of the embedding PDE (3) gives a solution of the original PDE (1) for every multi-dimensional phase-shift ϕ of the heterogeneity.

In particular, the field $u_0(t, x)$ satisfies the given heterogeneous PDE (1). \square

Lemma 2 (converse). *Suppose we have a set of solutions $u_\phi(t, x)$ of the phase-shifted PDE (4)—a set parametrised by the phase vector ϕ —and the set depends smoothly upon t, x, ϕ . Then the field $\mathbf{u}(t, x, x_1, x_2) := u_{(x_1-x, x_2-x)}(t, x)$ satisfies the embedding PDE (3).*

Proof. First, from the PDE (3), consider

$$\frac{\partial \mathbf{u}}{\partial x_0} + \frac{\partial \mathbf{u}}{\partial x_1} + \frac{\partial \mathbf{u}}{\partial x_2} = -\frac{\partial u_\phi}{\partial \phi_1} - \frac{\partial u_\phi}{\partial \phi_2} + \frac{\partial u_\phi}{\partial x} + \frac{\partial u_\phi}{\partial \phi_1} + \frac{\partial u_\phi}{\partial \phi_2} = \frac{\partial u_\phi}{\partial x}.$$

Second, since $\phi_i = x_i - x$, that is $x_i = x + \phi_i$, then

$$\left(\frac{\partial}{\partial x_0} + \frac{\partial}{\partial x_1} + \frac{\partial}{\partial x_2} \right) \kappa(x_1, x_2) = \frac{\partial}{\partial x} \kappa(x + \phi_1, x + \phi_2).$$

Thirdly, hence the right-hand-side of PDE (3) becomes

$$\begin{aligned}
& \left(\frac{\partial}{\partial x_0} + \frac{\partial}{\partial x_1} + \frac{\partial}{\partial x_2} \right) \left\{ \kappa(x_1, x_2) \frac{\partial u_\phi}{\partial x} \right\} \\
&= \frac{\partial}{\partial x} \kappa(x + \phi_1, x + \phi_2) \frac{\partial u_\phi}{\partial x} + \kappa(x_1, x_2) \left(\frac{\partial}{\partial x_0} + \frac{\partial}{\partial x_1} + \frac{\partial}{\partial x_2} \right) \frac{\partial u_\phi}{\partial x} \\
&= \frac{\partial}{\partial x} \kappa(x + \phi_1, x + \phi_2) \frac{\partial u_\phi}{\partial x} + \kappa(x + \phi_1, x + \phi_2) \frac{\partial^2 u_\phi}{\partial x^2} \\
&= \frac{\partial}{\partial x} \left\{ \kappa(x + \phi_1, x + \phi_2) \frac{\partial u_\phi}{\partial x} \right\},
\end{aligned}$$

the right-hand side of PDE (4). Lastly, since $\partial \mathbf{u} / \partial t = \partial u_\phi / \partial t$ it follows that $\mathbf{u} := u_{(x_1-x, x_2-x)}(t, x)$ satisfies the embedding PDE (3). \square

Corresponding results to Lemmas 1 and 2 hold for the heterogeneous wave PDE $u_{tt} = \partial_x \{ \kappa(x) u_x \}$, with ∂_t replaced by ∂_{tt} .

Consequently, PDEs (3) and (4) are equivalent, and they may provide us with a set of solutions for an ensemble of materials all with the same heterogeneity structure, but with the structural phase of the material shifted through all possibilities. The key difference between PDEs (3) and (4) is that although (4) is heterogeneous in space x , the embedding PDE (3) is *homogeneous* in x_0 . Because of this homogeneity, Section 3 is empowered to apply a rigorous theory for slow variations in space that leads to the desired homogenized PDE.

3 The slow manifold of homogenization

Let's analyse the embedding PDE (3) for a useful slow manifold. This slow manifold expresses and supports the emergence of a precise homogenization of the original heterogeneous PDE (1). Since the PDEs herein are linear, the slow manifold is more specifically a slow subspace, but I use the term *manifold* as the same framework and theory immediately also applies to cognate nonlinear systems.

Rigorous theory (Roberts 2015a) inspired by earlier formal arguments (Roberts 1988, 1997) establishes how to create a PDE model for the macroscale spatial structure of PDE solutions in cylindrical domains \mathcal{D} like Figure 1. The technique is to base analysis on the case where variations in x_0 are approx-

imately negligible, and then treat slow, macroscale, variations in x_0 as a regular perturbation (Roberts 2015b, Part III).¹²

The analysis proceeds to any chosen order N in the ‘small’ derivatives in x_0 . For two examples, the usual leading order homogenizations are the case $N = 2$, and the so-called second-order homogenizations¹³ correspond to the higher-order $N = 4$. To ensure the required derivatives and operators exist and have requisite properties, we analyse the systems in Sobolov spaces $\mathbb{H}_D := W^{N+1,2}(D)$ for various spatial domains D .

To establish the basis of a slow manifold, consider PDE (3), in the Sobolov space \mathbb{H}_D , with $\partial/\partial x_0$ neglected:

$$\frac{\partial \mathbf{u}}{\partial t} = \left(\frac{\partial}{\partial x_1} + \frac{\partial}{\partial x_2} \right) \left\{ \kappa(x_1, x_2) \left(\frac{\partial \mathbf{u}}{\partial x_1} + \frac{\partial \mathbf{u}}{\partial x_2} \right) \right\}, \quad (5)$$

to be solved with ℓ_i -periodic boundary conditions in x_i . The basis applies at each and every x_0 . Hence at every x_0 we consider PDE (5) on the Sobolov space $\mathbb{H}_\mathcal{C}$ where \mathcal{C} is the x_1x_2 -cross-section of \mathcal{D} .

Equilibria A family of equilibria is $\mathbf{u}(t, x_1, x_2) = U$, constant in x_1, x_2 , for every U . This family, in $\mathbb{H}_\mathcal{C}$ for every x_0 , forms a subspace of equilibria \mathbb{E} .

3.1 Spectrum at each equilibrium

We explore the spectrum about every equilibria in \mathbb{E} as the spectrum is crucial in identifying the existence and properties of invariant manifolds. Since PDE (5) is linear, the perturbation problem is identical at every U , namely (5) itself.

Example 3. Consider the case where the heterogeneity κ is constant. In the vector space $\mathbb{H}_\mathcal{C}$, and upon defining wavenumbers $k_i := 2\pi/\ell_i$, a complete set of linearly independent eigenfunctions of the right-hand side of (5) are $e^{i(mk_1x_1+nk_2x_2)}$ for every integer m, n . The spectrum of eigenvalues is then $\lambda_{mn} := -\kappa(mk_1 + nk_2)^2$. This spectrum has one zero-eigenvalue and the rest are negative: $\lambda_{mn} \leq -\kappa k_1^2 < 0$ (recall $\ell_1 > \ell_2$ so $k_1 < k_2$).

¹²Alternatively, in linear problems one could justify the analysis via a Fourier transform in x_0 (Roberts 1988, 2015b, §2 and Ch.7 resp.). However, for nonlinear problems it is better to analyse in physical space, so we do so herein—except for Section 5.

¹³(e.g., Anthoine 2010, Cornaggia & Guzina 2020, Hii & El Said 2022)

For general heterogeneity κ , we here establish that the eigenvalue problem associated with (5) is self-adjoint and hence has only real eigenvalues. Denote the right-hand side operator as $\mathcal{L}_0 := (\partial_{x_1} + \partial_{x_2})\{\kappa(x_1, x_2)(\partial_{x_1} + \partial_{x_2})\}$ to be solved with ℓ_i -periodic boundary conditions in x_i . Also, we use the inner product $\langle \mathbf{u}, \mathbf{v} \rangle := \iint_{\mathcal{C}} \mathbf{u} \bar{\mathbf{v}} dx_1 dx_2$ over the rectangular cross-section $\mathcal{C} := [0, \ell_1] \times [0, \ell_2]$, where an overbar denotes complex conjugation. Then, for every pair of functions $\mathbf{u}, \mathbf{v} \in \mathbb{H}$, consider

$$\begin{aligned} \langle \mathcal{L}_0 \mathbf{u}, \mathbf{v} \rangle &= \iint_{\mathcal{C}} \bar{\mathbf{v}} (\partial_{x_1} + \partial_{x_2}) \{ \kappa(\mathbf{u}_{x_1} + \mathbf{u}_{x_2}) \} dx_1 dx_2 \\ &= \iint_{\mathcal{C}} \bar{\mathbf{v}} \partial_{x_1} \{ \kappa(\mathbf{u}_{x_1} + \mathbf{u}_{x_2}) \} + \bar{\mathbf{v}} \partial_{x_2} \{ \kappa(\mathbf{u}_{x_1} + \mathbf{u}_{x_2}) \} dx_1 dx_2 \\ &= \int_0^{\ell_2} [\bar{\mathbf{v}} \kappa(\mathbf{u}_{x_1} + \mathbf{u}_{x_2})]_0^{\ell_1} - \int_0^{\ell_1} \bar{\mathbf{v}}_{x_1} \kappa(\mathbf{u}_{x_1} + \mathbf{u}_{x_2}) dx_1 dx_2 \\ &\quad + \int_0^{\ell_1} [\bar{\mathbf{v}} \kappa(\mathbf{u}_{x_1} + \mathbf{u}_{x_2})]_0^{\ell_2} - \int_0^{\ell_2} \bar{\mathbf{v}}_{x_2} \kappa(\mathbf{u}_{x_1} + \mathbf{u}_{x_2}) dx_2 dx_1 \\ &= - \iint_{\mathcal{C}} (\bar{\mathbf{v}}_{x_1} + \bar{\mathbf{v}}_{x_2}) \kappa(\mathbf{u}_{x_1} + \mathbf{u}_{x_2}) dx_1 dx_2 \end{aligned}$$

as the boundary contributions vanish due to the ℓ_i -periodicity. Reverse the above steps with the roles of \mathbf{u} and \mathbf{v} swapped, to then deduce $\langle \mathcal{L}_0 \mathbf{u}, \mathbf{v} \rangle = \langle \mathbf{u}, \mathcal{L}_0 \mathbf{v} \rangle$. Thus the operator \mathcal{L}_0 is self-adjoint.

Consequently every eigenvalue is real, and the eigenvectors are pairwise orthogonal (or may be chosen to be so).

The next step is to establish that all the non-zero eigenvalues of \mathcal{L}_0 are negative and bounded away from zero. Consider the eigen-problem $\mathcal{L}_0 \mathbf{v} = \lambda \mathbf{v}$ for cross-sectional structures $\mathbf{v} \in \mathbb{H}_{\mathcal{C}}$. Apply $\langle \cdot, \mathbf{v} \rangle$ to the eigen-problem to see

$$\begin{aligned} \lambda \langle \mathbf{v}, \mathbf{v} \rangle &= \iint_{\mathcal{C}} \bar{\mathbf{v}} (\partial_{x_1} + \partial_{x_2}) \{ \kappa(\mathbf{v}_{x_1} + \mathbf{v}_{x_2}) \} dx_1 dx_2 \\ &= \dots = - \iint_{\mathcal{C}} \kappa |\mathbf{v}_{x_1} + \mathbf{v}_{x_2}|^2 dx_1 dx_2 \\ &\leq -\kappa_{\min} \iint_{\mathcal{C}} |\mathbf{v}_{x_1} + \mathbf{v}_{x_2}|^2 dx_1 dx_2, \end{aligned}$$

via integration by parts, and the ℓ_i -periodic conditions in x_i . To deduce an upper bound on the non-zero eigenvalues λ , let's minimise $\iint_{\mathcal{C}} |\mathbf{v}_{x_1} + \mathbf{v}_{x_2}|^2 dx_1 dx_2$ subject to $\langle \mathbf{v}, \mathbf{v} \rangle = \iint_{\mathcal{C}} |\mathbf{v}|^2 dx_1 dx_2 = 1$ and that $\mathbf{v}(x_1, x_2)$ has zero mean (being orthogonal to the constant eigenvector corresponding to $\lambda = 0$).

Introduce a Lagrange multiplier μ , and use calculus of variations to minimise $\iint_{\mathcal{C}} |\mathbf{v}_{x_1} + \mathbf{v}_{x_2}|^2 dx_1 dx_2 + \mu (\iint_{\mathcal{C}} |\mathbf{v}|^2 dx_1 dx_2 - 1)$. Via integration by parts, it follows that a minimiser must satisfy $(\partial_{x_1} + \partial_{x_2})^2 \mathbf{v} = -\mu \mathbf{v}$ over $\mathbf{v} \in \mathbb{H}_{\mathcal{C}}$. This is the problem [Example 3](#) solved, giving potential minimisers as $e^{i(mk_1x_1+nk_2x_2)}$ for multiplier $\mu = (mk_1 + nk_2)^2$. The zero mean condition requires at least one of m, n non-zero, and since $\ell_1 > \ell_2$, so minima are thus linear combinations of $e^{imk_1x_1}$ for $m = \pm 1$. These give $\iint_{\mathcal{C}} |\mathbf{v}_{x_1} + \mathbf{v}_{x_2}|^2 dx_1 dx_2 / \langle \mathbf{v}, \mathbf{v} \rangle = k_1^2 = 4\pi^2/\ell_1^2$. Hence we obtain the upper bound on the non-zero eigenvalues of $\lambda \leq -\beta_1$ for $\beta_1 := 4\pi^2\kappa_{\min}/\ell_1^2$.

In the case of the heterogeneous wave propagation problem, $u_{tt} = \partial_x\{\kappa(x)u_x\}$, this subsection's eigenvalue analysis establishes that for the cross-sectional dynamics there exists a zero eigenvalue separated from pure imaginary eigenvalues of magnitude at least $\sqrt{\beta_1} = 2\pi\sqrt{\kappa_{\min}}/\ell_1$.

3.2 Results of slowly varying theory

Let's comment the preconditions for the next [Proposition 4](#) as listed in Assumption 2 of [Roberts \(2015a\)](#). First, [Section 3.1](#) establishes that the spectrum of \mathcal{L}_0 is as required for the Hilbert space $\mathbb{H}_{\mathcal{C}}$. Hence we decompose the space into two closed \mathcal{L}_0 -invariant subspaces, the centre \mathbb{E}_c^0 and the stable \mathbb{E}_s^0 . Since the operator \mathcal{L}_0 is self-adjoint it generates the required strongly continuous semigroups in the Sobolev space $\mathbb{H}_{\mathcal{C}}$ (e.g., [Carr 1981](#), Ch.6). Hence the following result holds for homogenization.

Proposition 4 (homogenized PDE). *By [Proposition 6](#) of [Roberts \(2015a\)](#), for every chosen truncation order N , in a domain \mathbb{X} of 'slowly varying solutions', and after the decay of transients $\mathcal{O}(e^{-\beta't})$ for $\beta' \approx \beta_1$, the mean field $U(t, x) := (\ell_1\ell_2)^{-1} \iint_{\mathcal{C}} \mathbf{u}(t, x, x_1, x_2) dx_1 dx_2$ satisfies a generalised homogeneous PDE*

$$\frac{\partial U}{\partial t} = \sum_{n=0}^N K_n \frac{\partial^n U}{\partial x^n}, \quad x \in \mathbb{X} \subset [0, L], \quad (6)$$

in terms of some deterministic constants K_n , to a quantifiable error ([Roberts 2015a](#), (9)–(10) and (23), resp.).

The above mentioned error (23) (from [Roberts 2015a](#)) involves too many new parameters to meaningfully detail here—but typically the most important factor at each and every location $x = X$ is the $(N + 1)$ th derivative of \mathbf{u} in a spatial neighbourhood of X . The open subset \mathbb{X} of the domain $[0, L]$ is then that part of the domain where the error in (6) ([Roberts 2015a](#),

eqn. (23)), dominantly $\partial_x^{N+1}\mathbf{u}$, is small enough for the modelling purposes at hand. Also, using the specific mean field defined in [Proposition 4](#)—the usual ‘cell average’—is optional: one may instead parametrise the macroscale slow manifold in terms of any reasonable alternative amplitude (e.g., [Roberts 2015b](#), §5.3.3).

A generating function argument ([Roberts 2015a](#), Corollaries 12 and 13) establishes that classic, formal, ‘slowly varying’ analyses of the embedding PDE (3) are valid. One just needs to formally treat derivatives in the ‘large’ direction, $\partial/\partial x_0$, as ‘small’ in a consistent asymptotic sense (e.g., [Roberts 1988, 1997](#)).

In the case of the heterogeneous wave propagation problem, $u_{tt} = \partial_x\{\kappa(x)u_x\}$, I conjecture that a backward theory ([Roberts 2022, Hochs & Roberts 2019](#)) approach to the slowly varying theory here would support a cognate version of [Proposition 4](#) about the generalised homogenous wave PDE $U_{tt} = \sum_{n=0}^N K_n \partial_x^n U$ describing its dispersive macroscale waves.

4 Example construction of homogenized PDE

Corollary 13 of [Roberts \(2015a\)](#) established that the procedure of [Roberts \(1988\)](#), previously viewed as formal, is indeed a rigorous way of constructing the slow manifold modelling PDEs (6). Here we use the computer algebra system (CAS) version of the procedure ([Roberts 1997](#)), as detailed in generality and examples of a book ([Roberts 2015b](#), Part III).

[Appendix A](#) lists and documents the computer algebra code. The code constructs the homogenization for the case of heterogeneity

$$\kappa(x_1, x_2) := 1/[1 + a_1 \cos k_1 x_1 + a_2 \cos k_2 x_2] \quad (7)$$

in terms of microscale wavenumbers $k_i := 2\pi/\ell_i$ for the given microscale periodicities ℓ_1, ℓ_2 . We write approximations to the slow manifold model of the embedding PDE (3) in terms of a ‘mean’ field $U(t, x)$ that evolves according to an homogenized PDE of the form (6).

Quickly verify an approximation First, [Appendix A.1](#) verifies that an approximate field is

$$\mathbf{u}(t, x, x_1, x_2) = U + (a_1/k_1 \sin k_1 x_1 + a_2/k_2 \sin k_2 x_2) \frac{\partial U}{\partial x}$$

$$+ (a_1/k_1^2 \cos k_1 x_1 + a_2/k_2^2 \cos k_2 x_2) \frac{\partial^2 U}{\partial x^2} + \dots \quad (8a)$$

such that the mean field U evolves according to the homogenized PDE

$$\frac{\partial U}{\partial t} = \frac{\partial^2 U}{\partial x^2} + \dots \quad (8b)$$

(the coefficient 1 of the mean diffusivity is the classic harmonic mean of the specific heterogeneous diffusivity (7)). To verify, substitute (8) into the governing PDE (3) and find the PDE's residual contains only terms in U_{xxx} and higher derivatives. We denote this by saying that the residual is zero to an error $\mathcal{O}(\partial_x^3)$. Since the PDE residual is $\mathcal{O}(\partial_x^3)$, then theory (Roberts 2015a, Prop. 6) assures us that the slow manifold (8) is correct to error $\mathcal{O}(\partial_x^3)$.

4.1 Iteration systematically constructs

To construct approximations systematically, we repeatedly compute the residual, which then drives corrections, until the residual is zero to the specified order of error. Theory then assures us the slow manifold is approximated to the same order of error (Roberts 2015a). For example, the CAS iteratively constructs the improved homogenization (the case $N = 6$) that

$$\begin{aligned} \frac{\partial U}{\partial t} = & \frac{\partial^2 U}{\partial x^2} + \frac{1}{2}(a_1^2/k_1^2 + a_2^2/k_2^2) \frac{\partial^4 U}{\partial x^4} \\ & + \left[\frac{1}{2}(a_1^2/k_1^2 + a_2^2/k_2^2)^2 - 2(a_1^2/k_1^4 + a_2^2/k_2^4) \right] \frac{\partial^6 U}{\partial x^6} + \mathcal{O}(\partial_x^7). \end{aligned} \quad (9)$$

The code of Appendix A.2 constructs this generalised homogenization (9), and executes in about 26 seconds. In the case of the heterogeneous wave propagation problem, $u_{tt} = \partial_x \{ \kappa(x) u_x \}$, we expect the macroscale homogenized dispersive wave PDE to have U_{tt} equal to the same right-hand side as the above.

In use, any specific truncation of higher-order homogenization, such as (9), may need some asymptotically consistent regularisation (e.g., Benjamin et al. 1972, §2). For an example of regularisation, let's suppose we choose the $N = 4$ truncation $U_t = U_{xx} + \alpha^2 U_{xxxx}$ with parameter $\alpha := \sqrt{(a_1^2/k_1^2 + a_2^2/k_2^2)}/2$. The fourth derivative term $+\alpha^2 U_{xxxx}$ is undesirably destabilising. But to the same order of error, namely $\mathcal{O}(\partial_x^6)$, the chosen truncation is asymptotically equivalent to the regularised equation $U_t = (1 - \alpha^2 \partial_x^2)^{-1} U_{xx}$. This regularisation may be alternatively written as

$$(1 - \alpha^2 \partial_x^2) U_t = U_{xx}, \quad \text{or} \quad U_t = \frac{1}{2\alpha} e^{-|x|/\alpha} \star U_{xx}. \quad (10)$$

The spatially nonlocal convolution $e^{-|x/\alpha|} \star$, whether explicit or implicit, stabilises the regularised chosen truncation while preserving asymptotic consistency (cf., [Mercer & Roberts 1994](#), §2.2). Such nonlocal PDEs have previously been found desirable in various homogenizations of heterogeneous systems (e.g., [Cooper 2018](#), pp.2–3).

Optional We may set $a_2 = 0$ to get simpler results for a single periodic component in the heterogeneity, namely $\kappa(x_1) = 1/[1 + a_1 \cos k_1 x_1]$. In this case it becomes feasible to construct the homogenization to high-order, $N = 34$, in spatial derivatives. To construct expressions that are exact in heterogeneity amplitude a_1 , we also need to construct to the same order in a_1 because the evidence is that here the expansions in homogeneity amplitude a_1 truncate at just less than the same order as the order of derivatives. For this option ([Appendix A.2](#)), the algebra of order $N = 34$ takes roughly one minute compute time.

In general The code of [Appendix A.2](#) assumes the heterogeneity $\kappa \approx 1$, specifically $\kappa = 1/[1 + \kappa']$ for some $\kappa' \propto a$. Then multiplication by κ is realised as multiplication by $\sum_{n=0}^{N-1} (-\kappa')^n$.

The method ([Roberts 1997](#)) is to start the iteration with the leading ‘trivial’ approximation for the field and its evolution: that is, $u \approx u^{(1)} := U$ such that $\partial U / \partial t \approx g^{(1)} := 0$. The n th iteration is given the approximations $u^{(n)}$ and $g^{(n)}$, and starts by evaluating, via the flux $f^{(n)} := -\kappa(u_x^{(n)} + u_{x_1}^{(n)} + u_{x_2}^{(n)})$, the residual of the embedding PDE (3):

$$\text{Res}^{(n)} := u_t^{(n)} + f_x^{(n)} + f_{x_1}^{(n)} + f_{x_2}^{(n)}.$$

First update the evolution via the solvability integral that here is the mean over x_1, x_2 : $g^{(n+1)} := g^{(n)} + g'$ where $g' := \overline{\text{Res}^{(n)}}$. Second, update the field by a correction u' through using two steps to solve $(\partial_{x_1} + \partial_{x_2})[\kappa(u'_{x_1} + u'_{x_2})] = \text{Res}^{(n)} + g'$: step 1 integrates to solve $v_{x_1} + v_{x_2} = \text{Res}^{(n)} + g'$ with zero mean to avoid unbounded updates; and step 2 integrates again to solve $u'_{x_1} + u'_{x_2} = v/\kappa$ with zero mean. This second “zero mean” ensures preservation of our *choice* that the macroscale field parameter U is to be the local mean of the microscale field u . Then update the field approximation with $u^{(n+1)} := u^{(n)} + u'$.

The iterative loop terminates when the PDE residual $\text{Res}^{(n)}$ is zero to the specified orders of error. Then the constructed homogenization, such as (8) and (9), is correct to the same order ([Roberts 2015a](#), Prop. 6).

Analogy with machine learning The recursive iteration used in the above construction was originally developed nearly 30 years ago (Roberts 1997). Let’s draw an analogy between this iteration and machine learning algorithms where an AI learns the generic form of the macroscale evolution from many thousands of simulations¹⁴. In the algorithm here, each recursive iteration is analogous to a layer in a deep neural network, evaluating residuals is analogous to a nonlinear neuronal function, the linear update corrections are analogous to using weighted linear combination of outputs of one layer as the inputs of the next layer. But here the recursion is a ‘smart neural network’ in that the neurones and the ‘linear weights’ are crafted to the problem at hand using the physics encoded in the PDE operator. Further, being analytic, a single analysis encompasses all ‘data points’ in the state space’s domain (here all ‘slowly varying’ functions in $\mathbb{H}_{\mathcal{D}}$), not just a finite sample as in machine learning (possibly a biased sample). Consequently, via such algorithms, I contend that mathematicians have for decades been using such recursive iteration for implementing smart analogues of machine learning. Such analytic learning empowers the physical interpretation, validation, and verification required by modern science (e.g. Brenner & Koumoutsakos 2021).

5 Spatial resolution of homogenization

An homogenized PDE, such as (6) and (9), accurately predicts the evolution of the mean field $U(t, x)$ *provided* that, on the scale of the heterogeneity, the spatial gradients are sufficiently small. That is, provided the solutions are sufficiently slowly varying in space. Matouš et al. (2017) [§3.2] phrased the proviso as “the scale of the microstructural fluctuations, $[\ell_1]$, must be ... much smaller than the macroscopic field fluctuations, ℓ_M ” (expressed similarly by Nguyen et al. 2011, §2.2.2). Question: what does “sufficiently small”, “sufficiently slowly varying”, or “much smaller” actually mean physically? This section provides an indicative *quantitative* answer.

Here we show that in a prototypical family of homogenization problems, we only need to require that the

$$\text{macroscale lengths } \ell_M \gtrsim 2\ell_1. \quad (11)$$

This lower bound on the macroscale lengths is approximate and indicative because the actual performance of an homogenization depends upon the details of the heterogeneity κ , a chosen truncation of the homogenized PDE,

¹⁴(e.g., González-García et al. 1998, Frank et al. 2020, Linot & Graham 2020)

any specific regularisation of the PDE, the desired error of predictions, and so on. But the numerical coefficient 2 in (11) arises from a well-established quantitative procedure.

The procedure we invoke is that of high-order construction followed by Domb–Sykes plots (e.g., [Domb & Sykes 1957](#), [van Dyke 1984](#)) and Mercer–Roberts plots ([Mercer & Roberts 1990](#), Appendix) that estimate the distance to the nearest, convergence limiting, singularity in series approximations. We analyse an homogenized PDE (6) and (9) by considering its corresponding Fourier transform ($\partial_x \leftrightarrow ik$): $\partial\tilde{U}/\partial t = \sum_{n=0}^{\infty} (ik)^n K_n \tilde{U}$ in terms of the Fourier transform $\tilde{U}(t, k)$ of the mean field $U(t, x)$. Then the coefficient $\mathcal{K}(k) := \sum_{n=0}^{\infty} (ik)^n K_n k^n$ is a series in wavenumber k . If we can show convergence for $|k| < k_*$ for some wavenumber bound k_* , then we deduce that the homogenized PDE is valid for spatial structures of length scale $\ell_M > 2\pi/k_*$. We know that the radius of convergence k_* is the distance to the singularity of $\mathcal{K}(k)$ nearest the origin ($k = 0$). But we only know N terms in the series for $\mathcal{K}(k)$, so Domb–Sykes and Mercer–Roberts plots estimate the distance k_* by extrapolating the ‘ratio test’ from finite n to infinity, in the cases of a single singularity or a complex conjugate pair of singularities, respectively. For example, this technique has been used to quantitatively predict the spatial limit on PDEs modelling shear dispersion in channels and pipes ([Mercer & Roberts 1990, 1994](#)). [Figure 2](#) is an example Mercer–Roberts plot for one homogenization case developed here. The extrapolations to $1/n = 0$ ($n \rightarrow \infty$) in the figure indicate that the convergence is limited by a complex conjugate pair of singularities at a distance in wavenumber space of $k_* \approx 1/\sqrt{3.6} \approx 0.52$.

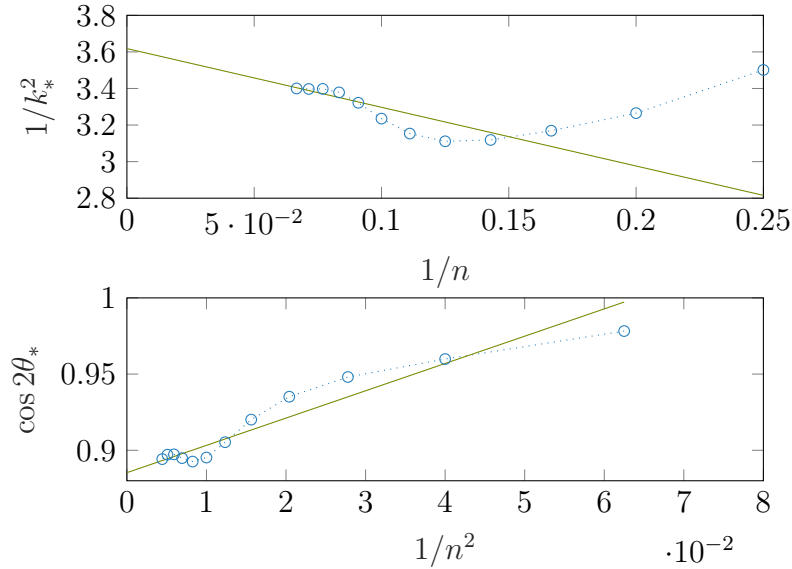
To obtain such plots and estimates we need to compute the homogenization series (6) and (9) to high-order. For the case of quasi-periodic heterogeneity the algebraic complexity explodes combinatorially with increasing order. Consequently, as a representative example, we explore the accessible case of homogenization with a single microscale period, specifically the heterogeneity

$$\kappa(x) := 1/[1 + a \cos x]. \quad (12)$$

The computer algebra code of [Section 4](#) constructs the homogenization in this case via the option of setting $a_2 = 0$, $a_1 = a$, and $k_1 = 1$. In this case the analysis is non-dimensionalised on the microscale length so that non-dimensionally $\ell_1 = 2\pi$. Executing the code with this option gives that the homogenized PDE (6) begins with

$$U_t = \left[\partial_x^2 + \frac{1}{2}a^2 \partial_x^4 + \left(-2a^2 - \frac{1}{2}a^4\right) \partial_x^6 + \left(8a^2 - \frac{135}{32}a^4 + \frac{5}{8}a^6\right) \partial_x^8 \right. \\ \left. + \left(-32a^2 + \frac{879}{32}a^4 - \frac{261}{32}a^6 + \frac{7}{8}a^8\right) \partial_x^{10} + \mathcal{O}(\partial_x^{12}) \right] U. \quad (13)$$

Figure 2: macroscale wavenumbers k of convergence are estimated from Mercer–Roberts plots (Mercer & Roberts 1990, Appendix) for the series $\mathcal{K}(k)$ in the case of heterogeneity (12), here with $a = 0.975$. We use the first 17 terms of the series in k^2 . Extrapolation to $1/n = 0$ estimates the location of a pair of complex conjugate singularities that limit the radius of convergence.

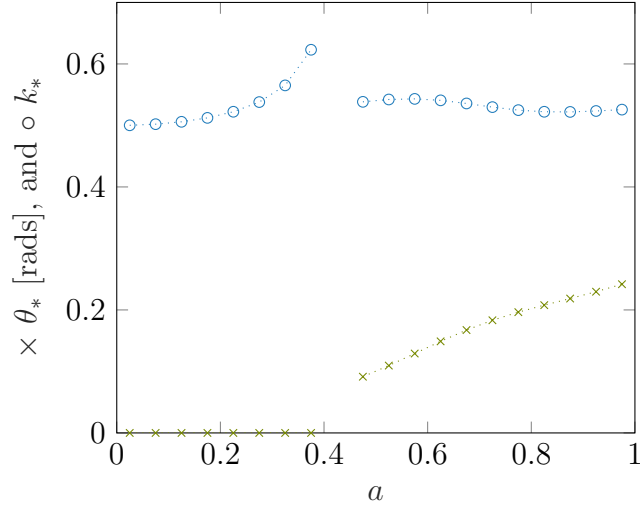


As a first step in investigating such high-order homogenization, observe that the a^2 terms are evidently all of the form $\frac{1}{2}a^2\partial_x^4(-4\partial_x^2)^{n/2-2}$ (this form holds up to at least order $n = 34$). Hence in Fourier space ($\partial_x \leftrightarrow ik$), the PDE (13) becomes the series for $\tilde{U}_t = [-k^2 + \frac{1}{2}a^2k^4/(1 - 4k^2) + \mathcal{O}(a^4)]\tilde{U}$. The divisor $(1 - 4k^2)$ in this expression indicates that, for small heterogeneity amplitude a , the wavenumbers resolvable by such an homogenization series are limited by the pole singularities at $k = \pm\frac{1}{2}$, that is, a bound on the convergence of the series is $k_* = 1/2$. Hence, for small a , the homogenized PDE (13) potentially resolves all wavelengths longer than $\ell_* := 2\pi/k_* = 4\pi = 2\ell_1$.¹⁵

I conjecture that the singularities at wavenumber $k = \pm\frac{1}{2}$ are connected to, in wave propagation through heterogeneous media, the well known phenomenon

¹⁵The limit $a \rightarrow 0$ is non-uniform. At $a = 0$ there is no heterogeneity and the ‘homogenized’ PDE (2) is precisely the original PDE (1) and therefore valid for *all* wavelengths and wavenumbers. Whereas for small non-zero a the singularities at wavenumber $k = \pm\frac{1}{2}$ persist and limit validity for small a —it is just that the singularities have a strength $\mathcal{O}(a^2)$ that vanishes as $a \rightarrow 0$.

Figure 3: In complex wavenumber space, plot estimates of the radius k_* (circles) and angle θ_* (crosses) of the convergence limiting singularity of the homogenization (13) as a function of the heterogeneity amplitude a in (12). The estimates around $a \approx 0.4$ are unreliable (see text).



of spectral gaps, namely frequencies at which no wave can propagate through the underlying medium (e.g., Cooper 2018, p.2).

Figure 3, for small a , confirms this bound on the wavenumbers and wavelengths. The estimates plotted in Figure 3 are obtained from Section 4 constructing the series (13) to errors of order 35 in ∂_x , or equivalently to errors $\mathcal{O}(k^{35})$. This CAS construction provides us with the first 17 non-zero coefficients in the series in k^2 for $\mathcal{K}(k)$.

- For heterogeneity amplitude $a \lesssim 0.4$ these coefficients have the same sign. Consequently, Domb–Sykes plots (e.g., Domb & Sykes 1957, van Dyke 1984), akin to the top panel of Figure 2, predict convergence limiting singularities at real $k = \pm k_*$ as shown in the left-part of Figure 3.
- For heterogeneity amplitude $a \gtrsim 0.4$ the coefficients have a more complicated sign pattern, indicating the convergence limiting singularity is now a complex conjugate pair in the complex k^2 -plane. Mercer–Roberts plots (Mercer & Roberts 1990, Appendix), such as Figure 2, estimate the radius and angle of these convergence limiting singularities as shown in the right-part of Figure 3.

The two distinct behaviours summarised in Figure 3 are likely due to singularities moving as a function of heterogeneity parameter a . We conjecture that for $a \lesssim 0.3$ there is a second real singularity for wavenumbers larger than the one at k_* . As a increases, both these singularities move and appear to collide for $a \approx 0.35$. After collision they separate and move out into the complex k plane ($a \gtrsim 0.4$). The Domb–Sykes and Mercer–Roberts estimates are

both unreliable near such collision, so the estimates for $a \approx 0.3$ to ≈ 0.4 are unreliable. With this caveat, the evidence of [Figure 3](#) indicates that across all $0 < a < 1$, our homogenization can resolve all wavenumbers $|k| < 1/2$. That is, high-order homogenization can resolve wavelengths longer than just twice the wavelength of the underlying periodicity.

In the case of the heterogeneous wave propagation problem, $u_{tt} = \partial_x\{\kappa(x)u_x\}$, we expect the same restrictions on the spatial resolution because we expect the right-hand side of PDE [\(9\)](#) to remain the same for the homogenized waves.

The case of quasi-periodic heterogeneity In the case of the quasi-periodic heterogeneity [\(7\)](#), observe in the homogenization PDE [\(9\)](#) that the coefficients in a_i are divided by wavenumbers k_i , and with increasing powers of k_i as the order increases. This indicates that higher-order terms in the series are dominated by the smallest wavenumber k_i , namely k_1 . That is, the higher-order terms should be dominated by the longest microscale heterogeneity, here that of $a_1 \cos(k_1 x)$. Hence we expect the limiting wavenumber and wavelengths to be the same as that for the single periodic heterogeneity [\(12\)](#). Consequently, expect the bound [\(11\)](#) to be valid for this quasi-periodic heterogeneity.

Temporal resolution The above exploration finds that the spatial resolution of the homogenization appears to vary little with heterogeneity strength a . The temporal resolution is quite a different issue, and it may depend significantly upon a . For example, [Figure 2](#) comes from the case $a = 0.975$ where the microscale heterogeneity varies by a factor of 80 across a microscale period. In similar scenarios, the time-scale of decay to the homogenized model, roughly $1/\beta_1 = \ell_1^2/(4\pi^2\kappa_{\min})$ (end of [Section 3.1](#)), may be several orders of magnitude longer than for small heterogeneity. For valid predictions by the homogenization, the macroscale time scale of interest needs to be longer than that of this decay.

In the case of the heterogeneous wave propagation problem, $u_{tt} = \partial_x\{\kappa(x)u_x\}$, the slow manifold is no longer attractive (unless there is some perturbing dissipative mechanism not included in this wave PDE). Instead we expect that the slow manifold acts as a ‘centre’ for any fast oscillations arising from the initial conditions. Indeed, conjectured backward theory (e.g., [Roberts 2022](#), §2.5) would more precisely assert that there is a system close to the PDE $u_{tt} = \partial_x\{\kappa(x)u_x\}$ (close to some specified order in some sense) that possesses a homogeneous slow manifold for the macroscale that acts as a

centre for all nearby dynamics. In this way the backward theory would establish accurate modelling over “timescales $\mathcal{O}(\varepsilon^{-\alpha})$ ” (Abdulle & Pouchon 2020, p.3), typically for exponent $\alpha = N$, the order of truncation.

6 Three-scale homogenization

There is interest in physical systems possessing a spatial microscale, a meso-scale, and a macroscale¹⁶. Such three-scale systems are encompassed in the framework of Section 2 when $\ell_2 \ll \ell_1 \ll L$. That is, the cylindrical domain of Figure 1 becomes like a physical ruler in that the domain is significantly thinner vertically than its width, and its width is significantly thinner than its length. Although Section 5 finds that these length ratios need to be at least two, they are not necessarily much bigger.

In this scenario, the arguments of Section 2 still apply: we solve the phase-shift embedding PDE (3) to obtain solutions of the heterogeneous PDEs (1) and (4). It is the slow manifold support and analysis that differs in detail.

Because this rigorous homogenization could in principal be exact at finite scale separation, we find here the expected result that a slow manifold homogenization of a ‘meso-slow’ manifold homogenization of the microscale system is the same as the slow manifold homogenization of the microscale (Sections 3 and 4). That is, this approach to homogenization is transitive in principal.

The same transitivity of homogenization would also hold in the case of the heterogeneous wave propagation problem, $u_{tt} = \partial_x \{ \kappa(x) u_x \}$.

6.1 Meso-slow homogenization

To analyse the heterogeneous PDEs (1) and (4) as a three-scale system we first establish and create the ‘meso-slow’ manifold homogenization. That is, we use that the domain \mathcal{D} , Figure 1, is thin in x_2 , that is $\ell_2 \ll \ell_1, L$. Consequently, we consider the embedding PDE (3) by assuming the spatial variations in both x_0 and x_1 are on a relatively large length scale. That is, the derivatives of \mathbf{u} and κ in both x_0 and x_1 are treated as small.

This homogenization is an example of that of a functionally graded material (e.g., Anthoine 2010) because the mesoscale variations in heterogeneity in x_1 are on a length scale $\ell_1 \gg \ell_2$. Our slow manifold approach systematically

¹⁶(e.g., Ramirez-Torres et al. 2018, Cruz-González et al. 2022)

incorporates all such variations within the analysis: for example, giving the fourth-order homogenization (16)–(17). At orders higher than the leading order, we systematically find higher-order derivatives of the larger scale material structure: for example, the fourth-order coefficient in the upcoming PDE (17) involves the third derivative $\mathfrak{K}'''(x_1)$ of the mesoscale variations. This approach automatically incorporates effects obtained by the “second-order homogenization” of Anthoine (2010).

Akin to Section 3, we here establish the basis of a slow manifold. Consider PDE (3), with $\partial/\partial x_0$ and $\partial/\partial x_1$ neglected, and in the Sobolov space $\mathbb{H}_{[0,\ell_2]}$ with ℓ_2 -periodic boundary conditions in x_2 :

$$\frac{\partial \mathbf{u}}{\partial t} = \frac{\partial}{\partial x_2} \left\{ \kappa(x_1, x_2) \frac{\partial \mathbf{u}}{\partial x_2} \right\}. \quad (14)$$

The basis established here applies at each and every x_0, x_1 .

Equilibria For PDE (14), and for every x_0, x_1 , in $\mathbb{H}_{[0,\ell_2]}$ clearly $\mathbf{u}(t, x_2) = \mathfrak{U}$, constant in x_2 , forms a subspace of equilibria \mathbb{E} .

Spectrum identifies invariant manifolds Since PDE (14) is linear, the perturbation problem is identical at every equilibria in \mathbb{E} , namely (14) itself. We need to characterise the right-hand side operator in (14), $\mathfrak{L}_0 := \partial/\partial x_2 \{ \kappa(x_1, x_2) \partial \cdot / \partial x_2 \}$ with ℓ_2 -periodic boundary conditions, in $\mathbb{H}_{[0,\ell_2]}$.

For example, in the case where the heterogeneity is constant with respect to x_2 , a complete set of linearly independent eigenfunctions of \mathfrak{L}_0 are $e^{in k_2 x_2}$ for every integer n . The spectrum of eigenvalues at (x_0, x_1) is then $\lambda_n(x_1) := -\kappa(x_1) k_2^2 n^2$. This spectrum has one zero-eigenvalue and the rest are negative: $\lambda_n(x_1) \leq -\kappa(x_1) k_2^2 < 0$. Hence, for every x_0, x_1 , the non-zero eigenvalues satisfy $\lambda_n(x_1) \leq -\kappa_{\min} k_2^2 < 0$.

For general heterogeneity, similar deductions to those of Section 3.1, establish that the operator \mathfrak{L}_0 is self-adjoint. Hence the eigenvalues are real, and eigenfunctions orthogonal. By a similar arguments to that of Section 3.1, it follows that the non-zero eigenvalues of the operator are bounded above by $\lambda \leq -\beta_2$ for $\beta_2 := \kappa_{\min} k_2^2 = 4\pi^2 \kappa_{\min} / \ell_2^2$.

Slowly varying theory We proceed analogous to Section 3.2 but now with two space dimensions (x_0 and x_1) in which solutions are slowly varying.

Roberts & Bunder (2017) developed rigorous slow manifold theory for spatio-temporal systems that have slow variations in multiple space dimensions. The operator \mathfrak{L}_0 satisfies the preconditions in Assumption 3 of Roberts & Bunder (2017) with one zero eigenvalue ($m = 1, \alpha = 0$) and the rest negative. By Proposition 1 of Roberts & Bunder (2017), and analogous to Proposition 4, we are assured that in a regime of slowly varying solutions, the mesoscale field $\mathfrak{U}(t, x_0, x_1)$ satisfies a PDE akin to (6), but in 2D space, to a quantified error (Roberts & Bunder 2017, eqn. (52)), and upon neglecting exponentially decaying transients (decaying faster than $e^{-\beta' t}$ for $\beta' \approx \beta_2$).

A generating function argument (Roberts & Bunder 2017, §§3.2–3.3) establishes the validity of formal ‘slowly varying’ analysis of the embedding PDE (3).

An example mesoscale homogenization Appendix B lists and describes CAS code to construct the mesoscale homogenization for the example case of heterogeneous diffusivity

$$\kappa(x_1, x_2) := 1/[1/\mathfrak{K}(x_1) + a_2 \cos k_2 x_2], \quad \text{for } k_2 := 2\pi/\ell_2, \quad (15)$$

and some given mesoscale heterogeneity function $\mathfrak{K}(x_1)$. The code derives that in terms of the mesoscale mean $\mathfrak{U}(t, x_0, x_1)$, and in terms of $\mathfrak{D}_x := \partial_{x_0} + \partial_{x_1}$, the microscale field (cf. (8a)) is

$$\mathfrak{u} = \mathfrak{U} + \frac{\mathfrak{K}(x_1)a_2 \sin k_2 x_2}{k_2} \mathfrak{D}_x \mathfrak{U} + \mathfrak{D}_x \left\{ \frac{\mathfrak{K}(x_1)a_2 \cos k_2 x_2}{k_2^2} \mathfrak{D}_x \mathfrak{U} \right\} + \mathcal{O}(\mathfrak{D}_x^3). \quad (16)$$

Simultaneously, the code derives that mesoscale mean field evolves according to the quasi-diffusion PDE

$$\frac{\partial \mathfrak{U}}{\partial t} = \mathfrak{D}_x \{ \mathfrak{K}(x_1) \mathfrak{D}_x \mathfrak{U} \} + \frac{a_2^2}{2k_2^2} \mathfrak{D}_x \{ \mathfrak{K}(x_1)^2 \mathfrak{D}_x^2 [\mathfrak{K}(x_1) \mathfrak{D}_x \mathfrak{U}] \} + \mathcal{O}(\mathfrak{D}_x^6). \quad (17)$$

As to be expected, the effective diffusivity on the mesoscale, $\mathfrak{K}(x_1)$, is the harmonic mean over x_2 of the microscale diffusivity (15). The theory of this subsection assures us that a truncation of the PDE (17) models the dynamics of the embedded PDE (3) whenever and wherever the spatial gradients in x_0 and x_1 are ‘small’ enough on the microscale ℓ_2 . That is, PDE (17) is a mesoscale model.

6.2 Homogenization of the mesoscale model

The mesoscale PDE (17) is heterogeneous on the spatial length scale ℓ_1 of variations in the coefficient $\mathfrak{K}(x_1)$. For the case $\ell_1 \ll L$ we here derive the macroscale homogenization of this mesoscale model. We have to choose some truncation of PDE (17) to analyse further, so let's choose the leading order truncation $\mathfrak{U}_t = \mathfrak{D}_x \{ \mathfrak{K}(x_1) \mathfrak{D}_x \mathfrak{U} \}$ as the mesoscale model.

To compare with the one-step homogenization, let's consider PDE (17) in the case where the mesoscale diffusivity is

$$\mathfrak{K}(x_1) := 1 / [1 + a_1 \cos k_1 x_1] \quad \text{for } k_1 := 2\pi / \ell_1. \quad (18)$$

The theory and construction of the homogenization follows the same procedure as detailed before, so let's just summarise here. First, we treat derivatives $\partial/\partial x_0$ as 'small'. Then the cross-sectional PDE is

$$\frac{\partial \mathfrak{U}}{\partial t} = \frac{\partial}{\partial x_1} \left\{ \mathfrak{K}(x_1) \frac{\partial \mathfrak{U}}{\partial x_1} \right\}, \quad (19)$$

to be solved with ℓ_1 -periodic boundary conditions in x_1 , and in space $\mathbb{H}_{[0, \ell_1]}$.

Second, a subspace of equilibria of (19) are $\mathfrak{U}(t, x_1) = U$, constant in x_1 . The spectrum of the linear operator $\mathcal{L}_0 := \partial/\partial x_1 \{ \mathfrak{K}(x_1) \partial/\partial x_1 \}$ can be shown to be self-adjoint with one zero eigenvalue and the rest negative and bounded away from zero, $\lambda \leq -\beta_1$, for $\beta_1 := k_1^2 \mathfrak{K}_{\min} = 4\pi^2 \mathfrak{K}_{\min} / \ell_1^2$.

Third, slowly varying theory for cylindrical domains, akin to Section 3.2, applies to assure us there exists a slow manifold homogenization of the mesoscale model in terms of a macroscale mean field $U(t, x_0)$. Further, the slow manifold emerges exponentially quickly on a time-scale of $1/\beta_1$, and we may approximate the slow manifold via formal 'slowly varying' analysis of the mesoscale PDE (17).

Fourth, the construction from the mesoscale PDE $\mathfrak{U}_t = \mathfrak{D}_x \{ \mathfrak{K}(x_1) \mathfrak{D}_x \mathfrak{U} \}$ to the macroscale homogenization is the specific case of Section 4 with $a_2 = 0$ and no variable x_2 . Consequently, corresponding results follow immediately, such as the slow manifold is (8a) with $a_2 = 0$, and the macroscale homogenization is $U_t = U_{xx}$ to errors $\mathcal{O}(\partial_x^4)$.

Here there is no point proceeding to higher order error in ∂_x because we chose the leading order mesoscale PDE at the start of this subsection. To obtain correct higher-order macroscale homogenizations, we would chose a correspondingly higher-order mesoscale homogenization.

7 Conclusion

This article further develops a novel theory and practice for mathematical/asymptotic homogenization to illuminate and resolve many issues in homogenization heterogeneous PDEs such as (1). [Section 2](#) invokes the technique of analysing an ensemble of all phase shifts, and extends it to multi-periodic cases, including the case of quasi-periodic. Future research may be able to extend the approach to interesting classes of random heterogeneity. The key to this approach is to be able to recast the ensemble as a system which is mathematically homogeneous in the macroscale.

Given a now mathematically homogeneous macroscale, [Section 3](#) applies recent developments of dynamical systems theory to newly establish the homogenization as a rigorous slow manifold of the given PDE system. No “ ϵ ” is required so the results hold for *finite* scale separation. No variational principles are required, so the approach applies to a wide range of physical problems, both dissipative and wave-like. The dynamical systems approach provides a framework that future research and applications may exploit to rigorously derive accurate initial conditions, boundary conditions, forcing projections, uncertainty evaluation, and error bounds.

This dynamical systems framework provides a very practical way to construct homogenized models, as in the example of [Section 4](#) and [Appendix A](#). It shows the ease in using computer algebra to perform and check the homogenization (8). The method systematically and straightforwardly extends to higher-order to derive so-called ‘second-order homogenization’: indeed, [Appendix A.2](#) simply proceeds further to explicitly construct the ‘fourth-order homogenization’ (9).

One advantage in the computer algebra is that, for some classes of heterogeneities, we can proceed to very high-order in the analysis. [Section 5](#) computed to 34th-order and uses the resulting generalised homogenization to quantify how ‘much smaller’ the microscale really has to be compared to the macroscale. Remarkably, the evidence is that, ideally, macroscale lengths can be resolved down to just twice the microscale length! Of course, in practice, there are many confounding aspects, but this factor of two is the mathematically ideal bound.

The spatio-temporal resolution of homogenizations could be improved, in future research, by multi-modal/multi-zonal homogenization of the heterogeneous microscale system by adapting approaches developed for shear dispersion ([Roberts & Struinin 2004](#), [Watt & Roberts 1995](#)).

Lastly, [Section 6](#) explores how the approach developed here includes the case when there are three separated length scales in the physical problem: a microscale, mesoscale, and macroscale. The exploration shows how one can analyse such a system in one step from the micro+mesoscale to the macroscale, or one can analyse the system in two steps from micro to meso, and then from meso to macro. Because sound modelling is transitive, the resulting homogenizations are the same. Further, if one's ultimate aim is a macroscale spatial discretisation in order to compute predictions, that is the aim is not really the homogenized PDE, then instead of the two step process of firstly homogenization and secondly spatial discretisation, future research could do it all in one step from microscale heterogeneous PDE to macroscale discretisation using a process like that introduced in a shear dispersion example ([MacKenzie & Roberts 2003](#)).

Acknowledgements I thank Arthur Norman and colleagues who maintain the computer algebra software Reduce. The Australian Research Council Discovery Project grants DP200103097 and DP220103156 helped support this research.

A Computer algebra to construct an homogenized PDE

The following code constructs the homogenization [\(6\)](#), discussed by [Section 4](#), of the PDEs [\(1\)](#) and [\(3\)](#) for the family of problems with diffusivity [\(7\)](#) for microscale periodicities ℓ_1, ℓ_2 . Let's use the computer algebra system Reduce¹⁷ as it is free, flexible, and fast ([Fateman 2003](#), e.g.). First improve printed output:

```
1 on div; off allfac; on revpri;
2 factor d,df;
```

Let the arguments of trig function heterogeneity be denoted by q_i and define wavenumbers $k_i := 2\pi/\ell_i$, so the diffusivity $\kappa(x_1, x_2)$ is the following.

```
3 depend q1,x1,z; depend q2,x2,z;
4 let { df(q1,x1)=>k1, df(q2,x2)=>k2 };
5 kappa:=1/(1+a1*cos(q1)+a2*cos(q2));
```

¹⁷<http://www.reduce-algebra.com>

Write approximations to the slow manifold model of the embedding PDE (3) in terms of a ‘mean’ field $U(t, x)$, denoted by `uu`, that evolves according to $\partial U/\partial t = \text{dudt}$ for whatever `dudt` happens to be.

```
6 depend uu, x, t;
7 let df(uu, t) => dudt;
```

This code uses x for x_0 as the two are synonymous in practice.

A.1 Quickly verify a leading approximation

First, we guess and then verify the approximate field (8a). This is coded, with ordering parameter `d` that counts the number of x -derivatives in U , as

```
8 u:=uu+d*(a1/k1*sin(q1)+a2/k2*sin(q2))*df(uu, x)
9      +d^2*(a1/k1^2*cos(q1)+a2/k2^2*cos(q2))*df(uu, x, 2);
```

such that U evolves according to the homogenized PDE $\partial U/\partial t = \partial^2 U/\partial x^2 + \dots$ (the coefficient 1 of the mean diffusivity is the classic harmonic mean of the specific heterogeneous diffusivity (7)):

```
10 dudt:=d^2*df(uu, x, 2);
```

To verify, substitute into the governing PDE (3) and find the PDE’s residual is zero to an error $\mathcal{O}(\partial_x^3)$ —counting the derivatives with the order parameter `d`.

```
11 let d^3=>0;
12 flux:=-kappa*(d*df(u, x)+df(u, x1)+df(u, x2))$
13 pde:=df(u, t)+d*df(flux, x)+df(flux, x1)+df(flux, x2);
```

Since the PDE residual is $\mathcal{O}(\partial_x^3)$, then the slow manifold (8a) is correct to error $\mathcal{O}(\partial_x^3)$ (Roberts 2015a).

The next subsection repeatedly computes the residual, to drive corrections, until the residual is zero to a specified order of error, and hence gives a slow manifold to the same order of error.

A.2 Iteration systematically constructs

Second, we iteratively construct the improved homogenization (9). This code executes in about four seconds.

```

14 write "
15 Second, Iteratively Construct
16 -----";

```

The terms $\mathcal{O}(\partial_x^4)$ appear, at first, impossible to find with exact algebra, so instead we construct in a power series in the amplitude of the heterogeneity. Let \mathbf{a} count the number of amplitude factors arising from κ . Choose the following order of errors in both derivatives and $a := \sqrt{a_1^2 + a_2^2}$. It eventuates that for this particular heterogeneity κ , the results to error $\mathcal{O}(\partial_x^{\text{ord}})$ appear exact in heterogeneity amplitude a .

```

17 ord:=7;

```

Here assume heterogeneity κ is a reciprocal, but could be more general.

```

18 rkappa:=sub({a1=a*a1,a2=a*a2},1/kappa);

```

Optional We may set $a_2 = 0$ to get simpler results for a single periodic component, and change truncation to the same order, now high-order. Order 35 takes roughly one minute compute time. The high-order coefficients of the homogenized PDE resulting from this option are exact, as far as they go, because the evidence is that the expansions in homogeneity amplitude a extend to at most the same order as the order of derivatives.

```

19 if 1 then begin a2:=0; a1:=k1:=1; ord:=35; end;

```

In general Construct heterogeneous diffusivity κ as the reciprocal of `rkappa`, presuming $\kappa \approx 1$:

```

20 kappa:=1+for n:=1:ord-1 sum (1-rkappa)^n$
21 res:=(kappa*rkappa-1 where a~~p=>0 when p>=ord);
22 if res neq 0 then rederr("kappa reciprocal error");

```

Start the iteration from the trivial approximation for the field and its evolution.

```

23 u:=uu;
24 dudt:=0;

```

Seek solution to the specified orders of errors.

```

25 for it:=1:999 do begin write "
26 **** ITERATION ",it;

```

Progressively truncate the order of the order parameter so that we control the residuals better: the bound in this if-statement is the aimed for ultimate order of error.

```

27 if it<ord then let {d^(it+1)=>0, a^(it+1)=>0};

```

Compute the PDE residual via the flux, trace printing the length of the residual expression:

```

28 flux:=-kappa*(d*df(u,x)+df(u,x1)+df(u,x2));
29 pde:=df(u,t)+d*df(flux,x)+df(flux,x1)+df(flux,x2);
30 pde:=trigsimp(pde,combine);
31 write lengthpde:=length(pde);

```

Update the evolution via the solvability condition from the mean over x_1, x_2 :

```

32 gd:=- (pde where {sin(~a)=>0,cos(~a)=>0});
33 if it<6 then write gd:=gd else write lengthgd:=length(gd);
34 dudt:=dudt+gd;
35 rhs:=pde+gd;

```

Attempt to solve the update in two steps, each step with two integrals. Use the following operator, given we already made q_i depend upon dummy z .

```

36 if it=1 then begin
37   operator intx; linear intx;
38   let { intx(cos(~q),z) => sin(q)/(df(q,x1)+df(q,x2))
39         , intx(sin(~q),z) =>-cos(q)/(df(q,x1)+df(q,x2))
40         };
41 end;

```

- First integrate $v_{x_1} + v_{x_2} = \text{rhs}$ with zero mean. If any $\text{intx}(1,z)$ appear then mistake.

```

42 v:=trigsimp( intx(rhs,z) );
43 if not freeof(v,intx(1,z)) then rederr("ABORT");

```

- Second, solve $\kappa u'_z = \kappa(u'_{x_1} + u'_{x_2}) = v$, using divide by κ and integrate again. Assume any presence of $\text{intx}(1,z)$ is an error that eventually

sorts itself out in the iteration, so obliterate here! The update then has mean zero.

```
44 ud:=intx(trigsimp(v*rkappa,combine),z);
45 ud:=(ud where intx(1,z)=>0);% obliterate
```

Add in the update. Perhaps trigsimp is useful here.

```
46 u:=u+trigsimp(ud);
```

Exit iterative for-loop when the PDE residual is zero

```
47 if pde=0 then write "Success: ", it:=it+10000;
48 end;
49 showtime;
50 if pde neq 0 then rederr("Iteration failure");
```

Write out homogenized PDE, optionally its coefficients, and end the script.

```
51 dudt:=dudt;
52 if ord>7 then begin cs:=coeff(dudt,d);
53   cs:=for n:=3 step 2 until length(cs)
54     collect part(cs,n)/df(uu,x,n-1);
55   on rounded; off nat; write cs:=cs;
56   on nat; off rounded; end;
57 end;
```

B Meso-scale homogenization code

Construct the asymptotic expansion of the meso-slow homogenization of three-scale diffusion supported by the theory of [Section 6.1](#).

```
58 on div; off allfac; on revpri;
59 factor d,b,a2,k2;
```

The diffusivity $\kappa(x_1, x_2)$ is the following, where $\mathbf{b}(n)$ denotes the n th derivative of $b(x_1)$. At the end we recast in $\mathbf{c} = \mathfrak{K}(x_1) := 1/b(x_1)$.

```
60 depend kappa,x1,x2;
61 operator b; depend b,x1;
62 kappa:=1/(b(0)+a2*cos(k2*x2));
63 let { df(b(~n),x1) => b(n+1) };
```

Write approximations to the slow manifold model of the embedding PDE (3) in terms of a ‘mean’ field $U(t, x)$ that evolves according to $\partial U / \partial t = \text{dudt}$.

```
64 depend uu, x, x1, t;
65 let df(uu, t) => dudt;
```

This code uses x for x_0 as the two are synonymous in practice. Start from the leading approximation for the field and its evolution.

```
66 u:=uu$
67 dudt:=0$
```

Iteratively construct to this order of error in slow derivatives.

```
68 ordd:=5;
69 for it:=1:999 do begin write "
70 **** Iteration ", it;
```

Progressively truncate the order of the order parameter so that we better control the residuals.

```
71 if it < ordd then let d^(it+1) => 0;
```

Compute the PDE residual via the flux, trace printing the length of the residual expression:

```
72 flux:=-kappa*(d*df(u, x)+d*df(u, x1)+df(u, x2));
73 pde:=df(u, t)+d*df(flux, x)+d*df(flux, x1)+df(flux, x2);
74 pde:=trigsimp(pde);
75 write lengthpde:=length(pde);
```

Solvability updates the evolution:

```
76 dudt:=dudt+(gd:=-int(pde, x2, 0, 2*pi/k2)/(2*pi/k2));
```

Update the field via some integrals:

```
77 ud:=trigsimp(int(int(pde+gd, x2)/kappa, x2));
78 udx:=sub(x2=2*pi/k2, ud)-sub(x2=0, ud);
79 u:=u+ud-int(ud, x2, 0, 2*pi/k2)/(2*pi/k2)
80 -udx*(x2-pi/k2+a2/k2/b(0)*sin(k2*x2))/(2*pi/k2);
```

Exit iterative for-loop when the residual is zero

```
81 showtime;
82 if pde=0 then write "Success: ", it:=it+10000;
83 end;
84 if pde neq 0 then rederr("Iteration failure");
```

Write out homogenized PDE.

```
85 dudt:=dudt;
```

Recast in terms of $c = \mathfrak{K}(x_1) := 1/b(x_1)$.

```
86 operator c; depend c,x1; factor c;
87 let { df(c(~n),x1)=>c(n+1), b(~n)=>df(1/c(0),x1,n) };
88 dudt:=dudt;
```

Check compact form of the evolution PDE, and finish the script.

```
89 procedure dx(a); d*(df(a,x)+df(a,x1))$
90 err:=- (dudt where d^5=>0) +dx(c(0)*dx(uu))
91   +a2^2/k2^2/2*dx(c(0)^2*dx(dx(c(0)*dx(uu)));
92 if err neq 0 then rederr("simplification failure");
93 end;
```

References

- Abdulle, A. & Pouchon, T. (2020), ‘Effective Models and Numerical Homogenization for Wave Propagation in Heterogeneous Media on Arbitrary Timescales’, *Foundations of Computational Mathematics* .
- Altmann, R., Henning, P. & Peterseim, D. (2021), ‘Numerical homogenization beyond scale separation’, *Acta Numerica* **30**, 1–86.
- Anthoine, A. (2010), ‘Second-order homogenisation of functionally graded materials’, *International Journal of Solids and Structures* **47**(11), 1477–1489.
- Barchiesi, E., Eugster, S. R., dell’Isola, F. & Hild, F. (2020), ‘Large in-plane elastic deformations of bi-pantographic fabrics: asymptotic homogenization and experimental validation’, *Mathematics and Mechanics of Solids* **25**(3), 739–767.

- Benjamin, T. B., Bona, J. L. & Mahony, J. J. (1972), ‘Model equations for long waves in nonlinear dispersive systems’, *Phil. Trans. R. Soc. Lond. A* **272**(1220), 47–78.
<http://rsta.royalsocietypublishing.org/content/272/1220/47>
- Birch, D. A. & Young, W. R. (2006), ‘A master equation for a spatial population model with pair interactions’, *Theoretical Population Biology* **70**, 26–42.
<http://dx.doi.org/10.1016/j.tpb.2005.11.007>
- Brenner, M. P. & Koumoutsakos, P. (2021), ‘Editorial: Machine Learning and Physical Review Fluids: An Editorial Perspective’, *Physical Review Fluids* **6**(7), 070001.
- Brown, D., Popov, P. & Efendiev, Y. (2011), ‘On homogenization of Stokes flow in slowly varying media with applications to fluid–structure interaction’, *GEM - International Journal on Geomathematics* pp. 1–25.
- Carr, J. (1981), *Applications of centre manifold theory*, Vol. 35 of *Applied Math. Sci.*, Springer–Verlag.
<http://books.google.com.au/books?id=93BdN7btys0C>
- Chen, C., Roberts, A. J. & Bunder, J. E. (2014), The macroscale boundary conditions for diffusion in a material with microscale varying diffusivities, in M. Nelson, T. Hamilton, M. Jennings & J. Bunder, eds, ‘Proceedings of the 11th Biennial Engineering Mathematics and Applications Conference, EMAC-2013’, Vol. 55 of *ANZIAM J.*, pp. C218–C234.
- Chen, C., Roberts, A. J. & Bunder, J. E. (2015), Macroscale boundary conditions for a non-linear heat exchanger, in J. Sharples & J. Bunder, eds, ‘Proceedings of the 17th Biennial Computational Techniques and Applications Conference, CTAC-2014’, Vol. 56 of *ANZIAM J.*, pp. C16–C31.
- Chen, C., Roberts, A. J. & Bunder, J. E. (2018), ‘Boundary conditions for macroscale waves in an elastic system with microscale heterogeneity’, *IMA Journal of Applied Mathematics* **83**(3), 1–33.
<http://arxiv.org/abs/1603.06686>
- Cooper, S. (2018), ‘Quasi-periodic two-scale homogenisation and effective spatial dispersion in high-contrast media’, *Calculus of Variations and Partial Differential Equations* **57**(3#76), 1–33.
- Cornaggia, R. & Guzina, B. B. (2020), ‘Second-order homogenization of boundary and transmission conditions for one-dimensional waves in periodic media’, *International Journal of Solids and Structures* **188–9**, 88–102.

- Cox, S. M. & Roberts, A. J. (1995), ‘Initial conditions for models of dynamical systems’, *Physica D* **85**, 126–141.
- Craster, R. V. (2015), Dynamic homogenization, in V. V. Mityushev & M. Ruzhansky, eds, ‘Analytic Methods in Interdisciplinary Applications’, Vol. 116 of *Springer Proceedings in Mathematics and Statistics*, Springer, pp. 41–50.
- Cruz-González, O. L., Ramirez-Torres, A., Rodriguez-Ramos, R., Penta, R. & Lebon, F. (2022), ‘Hierarchical heterogeneous one-dimensional problem in linear viscoelastic media’, *European Journal of Mechanics - A/Solids* **95**, 104617.
- Domb, C. & Sykes, M. F. (1957), ‘On the susceptibility of a ferromagnetic above the Curie point’, *Proc. Roy. Soc. Lond. A* **240**, 214–228.
- Drugan, W. J. & Willis, J. R. (1996), ‘A micromechanics-based nonlocal constitutive equation and estimates of representative volume element size for elastic composites’, *Journal of the Mechanics and Physics of Solids* **44**(4), 497–524.
- Engquist, B. & Souganidis, P. E. (2008), ‘Asymptotic and numerical homogenization’, *Acta Numerica* **17**, 147–190. doi:[10.1017/S0962492906360011](https://doi.org/10.1017/S0962492906360011).
- Fateman, R. (2003), ‘Comparing the speed of programs for sparse polynomial multiplication’, *ACM SIGSAM Bulletin* **37**(1), 4–15.
<http://www.cs.berkeley.edu/~fateman/papers/fastmult.pdf>
- Frank, M., Drikakis, D. & Charassis, V. (2020), ‘Machine-learning methods for computational science and engineering’, *Computation* **8**(15), 1–35.
- González-García, R., Rico-Martínez, R. & Kevrekidis, I. (1998), ‘Identification of distributed parameter systems a neural net based approach’, *Computers Chem. Engrg* **22**, S965–8.
- Gustafsson, B. & Mossino, J. (2003), ‘Non-periodic explicit homogenization and reduction of dimension: the linear case’, *IMA Journal of Applied Mathematics* **68**, 269–298.
- Hii, A. K. W. & El Said, B. (2022), ‘A kinematically consistent second-order computational homogenisation framework for thick shell models’, *Computer Methods in Applied Mechanics and Engineering* **398**, 115136.
- Hochs, P. & Roberts, A. J. (2019), ‘Normal forms and invariant manifolds for nonlinear, non-autonomous PDEs, viewed as ODEs in infinite dimensions’, *J. Differential Equations* **267**(12), 7263–7312.

- Klarmann, S., Gruttmann, F. & Klinkel, S. (2019), ‘Homogenization assumptions for coupled multiscale analysis of structural elements: beam kinematics’, *Computational Mechanics* .
- Linot, A. J. & Graham, M. D. (2020), ‘Deep learning to discover and predict dynamics on an inertial manifold’, *Phys. Rev. E* **101**(062209).
- MacKenzie, T. & Roberts, A. J. (2003), Holistic discretisation of shear dispersion in a two-dimensional channel, in K. Burrage & R. B. Sidje, eds, ‘Proc. of 10th Computational Techniques and Applications Conference CTAC-2001’, Vol. 44, pp. C512–C530.
- Matouš, K., Geers, M. G. D., Kouznetsova, V. G. & Gillman, A. (2017), ‘A review of predictive nonlinear theories for multiscale modeling of heterogeneous materials’, *Journal of Computational Physics* **330**, 192–220.
- Mercer, G. N. & Roberts, A. J. (1990), ‘A centre manifold description of contaminant dispersion in channels with varying flow properties’, *SIAM J. Appl. Math.* **50**, 1547–1565.
- Mercer, G. N. & Roberts, A. J. (1994), ‘A complete model of shear dispersion in pipes’, *Jap. J. Indust. Appl. Math.* **11**, 499–521.
- Nguyen, V. P., Stroeve, M. & Sluys, L. J. (2011), ‘Multiscale continuous and discontinuous modeling of heterogeneous materials: a review on recent developments’, *Journal of Multiscale Modelling* **03**(04), 229–270.
- Niyonzima, I. (2014), Multiscale Finite Element Modeling of Nonlinear Quasistatic Electromagnetic Problems, PhD thesis, Université de Liège, Faculté des Sciences Appliquées.
- Ramirez-Torres, A., Penta, R., Rodriguez-Ramos, R., Merodio, J., Sabina, F. J., Bravo-Castillero, J., Guinovart-Diaz, R., Preziosi, L. & Grillo, A. (2018), ‘Three scales asymptotic homogenization and its application to layered hierarchical hard tissues’, *International Journal of Solids and Structures* **130–131**, 190–198.
- Roberts, A. J. (1988), ‘The application of centre manifold theory to the evolution of systems which vary slowly in space’, *J. Austral. Math. Soc. B* **29**, 480–500.
- Roberts, A. J. (1989), ‘Appropriate initial conditions for asymptotic descriptions of the long term evolution of dynamical systems’, *J. Austral. Math. Soc. B* **31**, 48–75.

- Roberts, A. J. (1992), ‘Boundary conditions for approximate differential equations’, *J. Austral. Math. Soc. B* **34**, 54–80.
- Roberts, A. J. (1993), ‘The invariant manifold of beam deformations. part 1: the simple circular rod’, *J. Elas.* **30**, 1–54.
- Roberts, A. J. (1997), ‘Low-dimensional modelling of dynamics via computer algebra’, *Computer Phys. Comm.* **100**, 215–230.
- Roberts, A. J. (2000), ‘Computer algebra derives correct initial conditions for low-dimensional dynamical models’, *Computer Phys. Comm.* **126**(3), 187–206.
- Roberts, A. J. (2015a), ‘Macroscale, slowly varying, models emerge from the microscale dynamics in long thin domains’, *IMA Journal of Applied Mathematics* **80**(5), 1492–1518.
- Roberts, A. J. (2015b), *Model emergent dynamics in complex systems*, SIAM, Philadelphia.
<http://bookstore.siam.org/mm20/>
- Roberts, A. J. (2022), Backwards theory supports modelling via invariant manifolds for non-autonomous dynamical systems, Technical report, [<http://arxiv.org/abs/1804.06998>].
- Roberts, A. J. & Bunder, J. E. (2017), ‘Slowly varying, macroscale models emerge from microscale dynamics over multiscale domains’, *IMA Journal of Applied Mathematics* **82**, 971–1012.
<http://arxiv.org/abs/1612.02079>
- Roberts, A. J. & Strunin, D. V. (2004), ‘Two-zone model of shear dispersion in a channel using centre manifolds’, *Quart. J. Mech. Appl. Math.* **57**, 363–378.
- Romanazzi, P., Bruna, M. & Howey, D. (2016), ‘Thermal homogenisation of electrical machine windings applying the multiple-scales method’, *Journal of Heat Transfer* .
- Saeb, S., Steinmann, P. & Javili, A. (2016), ‘Aspects of Computational Homogenization at Finite Deformations: A Unifying Review From Reuss’ to Voigt’s Bound’, *Applied Mechanics Reviews* **68**(5).
- Schneider, M. (2021), ‘A review of nonlinear FFT-based computational homogenization methods’, *Acta Mechanica* **232**(6), 2051–2100.

- Shahraki, D. P. & Guzina, B. B. (2020), Homogenization of the wave equation with non-uniformly oscillating coefficients, Technical report, <http://arxiv.org/abs/2006.02550>.
- Somnic, J. & Jo, B. W. (2022a), ‘Homogenization Methods of Lattice Materials’, *Encyclopedia* **2**(2), 1091–1102.
- Somnic, J. & Jo, B. W. (2022b), ‘Status and challenges in homogenization methods for lattice materials’, *Materials* **15**(2), 605.
- van Dyke, M. (1984), ‘Computer-extended series’, *Annu. Rev. Fluid Mech.* **16**, 287–310.
- van Kampen, N. (1992), *Stochastic processes in physics and chemistry*, Elsevier.
- Watt, S. D. & Roberts, A. J. (1995), ‘The accurate dynamic modelling of contaminant dispersion in channels’, *SIAM J. Appl. Math.* **55**(4), 1016–1038. <http://epubs.siam.org/sam-bin/dbq/article/25797>.
- Welsh, Z., Simpson, M. J., Khan, M. I. H. & Karim, M. A. (2018), ‘Multi-scale modeling for food drying : State of the art’, *Comprehensive Reviews in Food Science and Food Safety* .
<https://onlinelibrary.wiley.com/doi/abs/10.1111/1541-4337.12380>